Straining Nanomembranes *via* Highly Mismatched Heteroepitaxial Growth: InAs Islands on Compliant Si Substrates

Christoph Deneke,[†,‡,*] Angelo Malachias,[§] Armando Rastelli,[‡,⊥] Leandro Merces,[†] Minghuang Huang,[∥,*] Francesca Cavallo,[∥] Oliver G. Schmidt,[‡] and Max G. Lagally[∥]

[†]Laboratório Nacional de Nanotecnologia (LNNano), Rua Giuseppe Máximo Scolfaro 10000, 13083-100 Campinas, SP, Brazil, [‡]Institute for Integrative Nanosciences, IFW Dresden, Helmholtzstraße 20, D-01069 Dresden, Germany, [§]Departamento de Física, Universidade Federal de Minas Gerais, CP 702, 30123-970 Belo Horizonte, MG, Brazil, [⊥]Institute of Semiconductor and Solid State Physics, Johannes Kepler University, Altenberger Straße 69, A-4040 Linz, Austria, and [∥]Department of Materials Science and Engineering, University of Wisconsin—Madison, 1500 Engineering Drive, Madison, Wisconsin 53706, United States

ABSTRACT Freestanding, edge-supported silicon nanomembranes are defined by selective underetching of patterned silicon-on-insulator substrates. The membranes are afterward introduced into a molecular beam epitaxy chamber and overgrown with InAs, resulting in the formation of InAs islands on flat areas and at the top of the Si nanomembranes. A detailed analysis of sample morphology, island structure, and strain is carried out. Scanning electron microscopy shows that the membrane stays intact during overgrowth. Atomic force microscopy reveals a lower island density on top of the freestanding membranes, denoting a modified wetting or diffusivity in these areas. An observed bending of the membrane indicates a strain transfer from the InAs islands to the compliant substrate. X-ray diffraction and finite-element modeling indicate a nonuniform strain state of the island ensemble grown on the freestanding membrane. A simulation of the bending of the nanomembranes indicates that the islands at the center of the freestanding area are highly strained, whereas islands on the border tend to be fully relaxed. Finally, continuum elasticity calculations suggest that for a sufficiently thin membrane InAs could transfer enough strain to the membrane to allow coherent epitaxial growth, something not possible on bulk substrates.

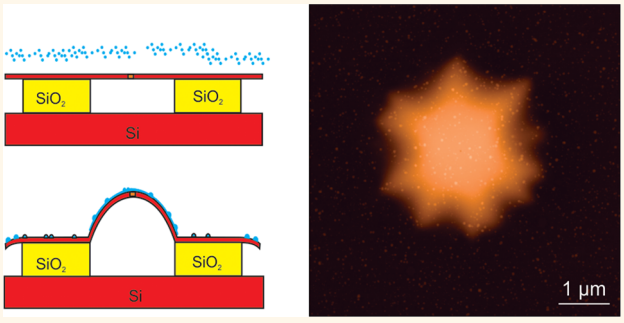

KEYWORDS: freestanding membranes · InAs on silicon · self-assembled growth · molecular beam epitaxy

Freestanding nanomembranes, single-crystalline semiconductor films with thickness in the range of 5 to 300 nm, but with macroscopic areas, have attracted considerable attention in recent years.[1−7] The fascination arises from the combination of an exceptional mechanical compliance with the properties of high-quality inorganic single crystals, which opened new possibilities for device tailoring. Structures and prototype devices that have been investigated include stretchable electronics,[8−11] solar cells,[12,13] high-speed silicon transistors,[6] photodetectors,[14] tunable single-photon emitters on piezoelectric substrates,[15] and metal-semiconductor field effect transistors,[16] as well as rolled-up or folded three-dimensional micro- and nano-objects.[17−20]

Recently, freestanding nanomembranes were used as substrates for self-assembled growth of Ge islands on silicon.[21−25] Hereby, the mechanical properties of the thin substrate, with thickness comparable to the nominal coverage with deposited material, give rise to fundamental changes in growth behavior.[24] In particular, strained Ge islands induce a large degree of local and global deformation in the Si nanomembrane substrate. The lattice deformation in the substrate in turn provides a feedback mechanism that alters growth conditions of Ge islands, in terms of ordering, density, size, and strain distribution in the islands.[21−25] Furthermore, the ability to induce a significant lattice distortion in the compliant substrate has important implications for applications, as

* Address correspondence to christoph.deneke@lnls.br, whaleson01@gmail.com.

Received for review September 9, 2012 and accepted October 9, 2012.

Published online October 09, 2012
10.1021/nn304151j

mechanical strain changes electronic properties of materials.[15,22,26,27] The influence of a compliant substrate on the growth behavior has triggered a series of experimental[21−24] and theoretical[25,28,29] studies for Ge on Si nanomembranes.

InAs (and other III−V materials) integration on Si has been extensively studied since the early 1980s because of the potential optoelectronic applications of the combination of the two materials. Among other issues, the large lattice misfit between InAs and Si (10.6%) as well as the high difference in thermal expansion coefficients make the growth of electronic- or optical-quality material challenging.[30−34] As epitaxial growth is strongly influenced by the lattice mismatch between two materials,[35] the use of a compliant substrate such as a Si nanomembrane could open a new possibility to tackle the problem. Starting from the work of Ge on Si, we expect that, on one hand, the InAs can transfer some of the strain arising from lattice mismatch and thermal expansion to the nanomembrane, providing a path toward coherent growth. On the other hand, the high lattice mismatch between InAs and Si allows a large amount of strain to be imparted in thin Si membranes by the InAs islands (nanostressors), giving rise to larger changes in the membrane electronic properties than in a membrane strained using Ge.

In this work, freestanding, but edge-attached silicon nanomembranes, made by selective underetching of patterned silicon-on-insulator (SOI) substrates, were overgrown with InAs by molecular beam epitaxy (MBE). The formation of InAs islands was observed already after deposition of a submonolayer of InAs by changes in the reflection high-energy electron diffraction (RHEED) pattern. The sample morphology after growth as well as the nanostructures that formed were investigated by different microscopy methods, and their strain state was characterized by X-ray diffraction (XRD). We found from scanning electron microscopy (SEM) as well as atomic force microscopy (AFM) that islands on the freestanding membranes have a lower density compared to the islands formed on the supported membrane. The bending of the freestanding parts upon strain relaxation of the InAs islands was observed by AFM and modeled by finite-element method (FEM) calculations for different distributions of interface strain between island and membrane as a function of island position on the freestanding membrane. Finally, continuum elasticity calculations show that a 3.5 nm thick Si membrane could accommodate enough strain of the InAs islands to allow fully coherent epitaxial growth of InAs on top of such a substrate.

RESULTS AND DISCUSSION

The sketches in Figure 1a−d illustrate the sample structure as well as the InAs growth process. Samples are patterned SOI substrates with a final silicon nanomembrane thickness of about 10, 15, and 20 nm.

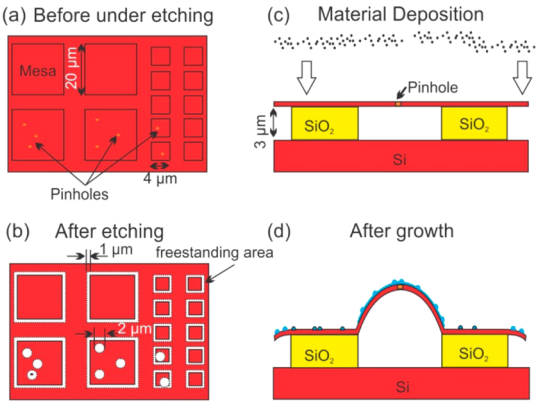

Figure 1. Schematic representation of the overgrown samples as well as the process flow. (a) Lithographically defined patterns on a SOI substrate with various lateral sizes. Note pinholes, which serve as channels for access of the etchant to the oxide release layer. (b) Underetching gives rise to two types of freestanding areas: (1) cantilevers emanating from edges of the mesas and (2) circular freestanding areas underneath pinholes in the ultrathin top Si layer of the SOI structure. (c) Prior to growth, freestanding membranes are defined by selective removal of the SiO_2 layer of a SOI wafer. (d) After InAs deposition, the strain transferred from the InAs islands gives rise to bending of the freestanding areas of nanomembranes.

Figure 1a depicts the sample after the lithography before underetching. Squared mesas are defined, which are then underetched to obtain freestanding areas (Figure 1b). The underetching gives rise to two types of freestanding regions: (1) the borders of the square mesa patterns, which become effectively cantilevered shelves, and (2) circular areas inside the sample where pinholes (localized defects) are present in the thin top Si layer, allowing the etchant to penetrate to the underlying SiO_2. Figure 1c depicts a side view of the sample before growth. Beside the cantilevers, round underetched areas on the mesa are present. After growth (Figure 1d), InAs islands form on all areas of the sample. For InAs, we expect a Volmer−Weber-like growth mode on the rigid parts of the substrate.[32] Therefore, we should observe no wetting of the substrate and 3D island formation already for submonolayer deposition. Indeed, a change of the RHEED pattern indicating 3D island formation was detected after 0.3 monolayer (ML) InAs deposition, as reported in the literature.[32]

The SEM images in Figure 2a and b provide a detailed look into the freestanding regions of the samples. The width of the freestanding part is about 1.2 μm for the edges (Figure 2a). For the same etching time, the diameter of the freestanding areas around pinholes (marked in Figure 2b) is about 2.4 μm (Figure 2b). On top of the whole Si layer, InAs islands can be identified (bright white spots). A visual inspection indicates that the island density is smaller on the freestanding areas compared to the areas still attached to the SiO_2 layer. These overview SEM images demonstrate that the patterned substrates are not damaged during cleaning, preparation, and overgrowth.

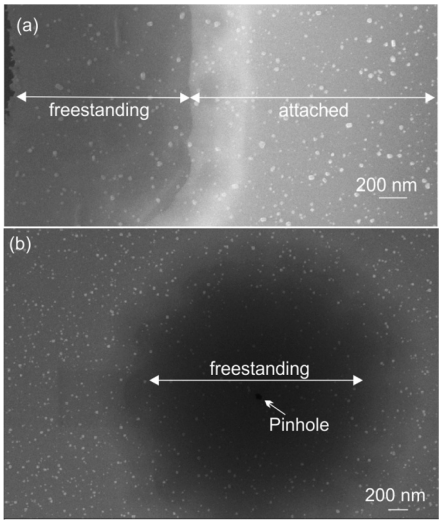

Figure 2. SEM images of InAs deposition on supported and unsupported regions of a Si nanomembrane. (a) One membrane border: freestanding as well as attached areas are depicted. (b) Image of a circular freestanding area obtained by SiO_2 etching through and below a pinhole. Both images show that the island density is lower on the freestanding than on the supported membrane.

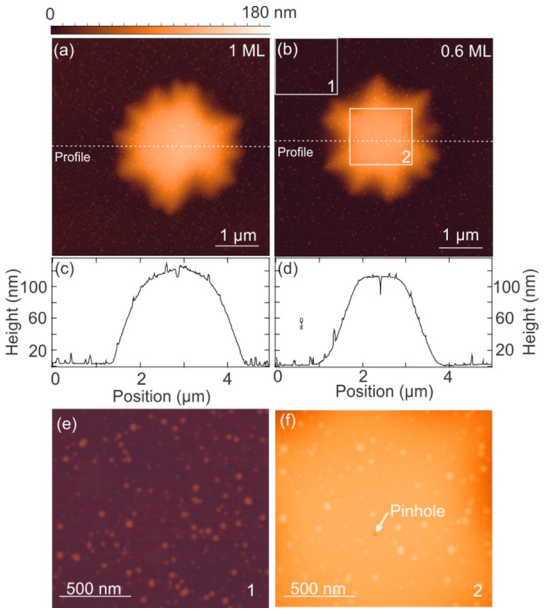

Figure 3. (a) AFM image of a freestanding area of a sample overgrown with 1 ML InAs. The height contours as well as the line scan profile (c) indicate a bending of the nanomembrane in the freestanding parts. (b and d) AFM image and a line scan profile of a sample with 0.6 ML InAs coverage, respectively. (e and f) Magnified areas of image (b). The images show a higher island density on the flat, rigid areas 1 compared to the areas of the freestanding membrane 2.

To obtain quantitative data about the deposited InAs islands, AFM images were collected around freestanding areas for two different samples with 1 and 0.6 ML InAs coverage (determined by the InAs growth rate and deposition time), respectively.

Figure 3a and b show two $5 \times 5\ \mu m^2$ AFM images for Si nanomembrane samples with 1 and 0.6 ML coverage of InAs. Line profiles crossing the middle of the bent areas are depicted (Figure 3c and d) to illustrate the bowing of the membranes. From the AFM image and the line profile, we can estimate the area of the freestanding membrane to be about 6.1 μm^2 with a diameter of about 2.8 μm for the sample with 1 ML InAs deposited. The shape and the line profile look slightly different for the 0.6 ML sample (Figure 3b and d), but the estimated area and diameter are very similar to the structure shown in Figure 3a (5.3 μm^2 and 2.6 μm, respectively). The line profiles in Figure 3c and d prove that the membrane bends more than 100 nm up in the center, indicating that the InAs islands can transfer some of their strain to the compliant substrate. The average strain at the membrane can be estimated by comparing its baseline (the diameter; considering no bending) to its length after bending that is quantified from AFM measurements. This simple calculation leads to an average strain of $\varepsilon_{Si} = 0.29\%$ for the values extracted from Figure 3b. The strain distribution in the nanomembrane is certainly inhomogeneous because the InAs 3D nanostressor islands have small size, are widely separated on the substrate, and have a spatially localized effect on the lattice.[25]

The bending was not observed in samples that had undergone the identical preparation and pregrowth procedure (see Methods for details) without InAs islands deposited. Also no wrinkling or bonding back to the substrate was observed for our samples, with or without the growth of islands.

A careful investigation of Figure 3a confirms the data shown in the SEM images of Figure 2, *i.e.,* that the InAs island density is smaller on the freestanding parts. This trend is also observed in Figure 3b for the lower InAs coverage and illustrated by the magnified areas depicted in Figure 3e and f. The island density is clearly smaller on the freestanding (Figure 3f) than in the supported areas (Figure 3e), and islands on the freestanding regions appear larger in diameter. Furthermore, the line profiles suggest island heights from 10 to 20 nm on the rigid as well as on the compliant areas of the sample. To quantify these observations, we performed image analysis to identify the islands and measure their height and density.[36] As we observe no special behavior of the border between attached and freestanding part, a mask was defined only containing the freestanding part, and analysis was carried out for these two regions of the sample.

In Figure 4 results of a statistical analysis of the identified islands are shown for the different areas of the samples. The island densities are derived from the total island number and the calculated areas in Figure 3b. For the freestanding area higher islands are observed and the shape of the height histogram (Figure 4a) is closer to a Gaussian normal distribution than the height histogram of the island on the rigid substrate (Figure 4b). The island density on the membrane

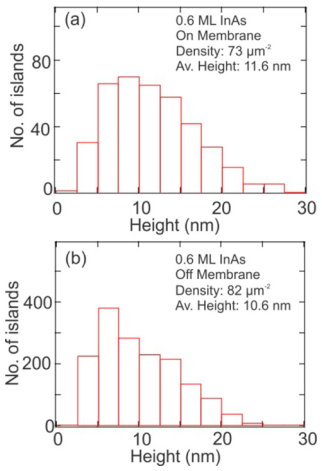

Figure 4. Statistical analysis of the height and density of the InAs islands for freestanding (on membrane) and rigid (off membrane) areas. Island heights on the freestanding areas are shifted to slightly larger values. The island density is slightly lower on the membranes compared to the surrounding area.

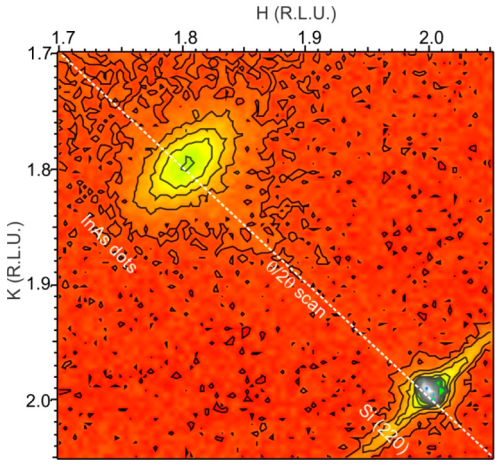

Figure 5. Reciprocal-space map in the vicinity of the Si (220) reflection for the sample with 1 ML InAs coverage. A narrow Si substrate peak (lower right) and an intense diffuse peak (upper left) ascribed to the InAs islands near the expected lattice parameter for bulk InAs are observed. The diffuse peak has a tail toward the Si peak, representing an ensemble of islands with lattice parameter smaller than that of bulk InAs. The white dotted line marks the path of the radial scan shown in Figure 6a.

is 73 μm^{-2}, whereas the density on the rigid area reaches 82 μm^{-2}, with a height difference of 11.6 nm (on membrane) to 10.6 nm (off membrane). As the total volume of deposited material is rather similar on the freestanding and the rigid areas, no preferential diffusion seems to take place from or to the freestanding membrane. Nevertheless, the change in island density and height distribution indicates a different island formation process on the freestanding membrane. Epitaxy processes are commonly dominated by attachment and diffusion of the deposited material; these two processes appear to differ on and off the freestanding parts of the nanomembrane. The shift to taller islands and the more symmetric height distribution point to a change in the diffusion on top of the freestanding membrane. Such a phenomenon in ultrathin freestanding substrates and its influence on the diffusion and wetting behavior of a deposited material were already observed for a chemically compatible system, Ge on Si.[24]

To evaluate the strain state of islands quantitatively, grazing-incidence X-ray diffraction (GI-XRD) measurements were carried out. Figure 5 shows a reciprocal-space map in the vicinity of the Si(220) reflection[37] for the sample with 1 ML InAs coverage. A similar result was obtained with the 0.6 ML sample. The map shows a narrow, intense peak at the Si(220) reciprocal-space position, coming from the substrate. Furthermore, a diffuse peak ascribed to the InAs islands is observed at the reciprocal-space position of (1.8, 1.8, 0), as expected for fully relaxed, hence dislocated InAs nanostructures. The peak shows an asymmetric tail toward the substrate position, which we attribute to the InAs islands on the freestanding membrane areas. This tail is the first evidence of an ensemble of islands exhibiting a different strain state. In order to investigate the strain state of these islands in greater detail, we performed radial (longitudinal) $\theta/2\theta$ scans along the line represented in Figure 5. Similar scans were performed for the 0.6 ML samples. Additionally, angular (transversal) scans were obtained at several positions in the vicinity of the InAs peak.

Figure 6a shows a radial $\theta/2\theta$ scan for the sample with 1 ML InAs coverage. Besides the sharp Si substrate peak one observes the diffuse scattering from InAs islands at lower (h,k) values (therefore larger lattice parameters). We can decompose this latter peak into two main contributions by fitting two Gaussian curves to the intensity profile [green solid and blue dashed lines in Figure 6a], which can describe the observed intensity profile (the sum of contributions is shown as a red dotted line). From the peak position we can calculate the in-plane lattice parameters for both contributions (6.038 and 5.995 Å) with an in-plane strain accuracy determination of about 0.05%.[38] The scattering from the nanomembrane area is weaker because the area of compliant substrate is much less than the bulk SOI areas. We find that the majority of islands that are related to the intense InAs peak are plastically relaxed (most likely with dislocations at the InAs/Si interface), having nearly the lattice parameter of bulk InAs.[32,34,39] Furthermore, the broader contribution and the relative peak areas (proportional to the volume of strained material) suggest a smaller number of InAs islands that exhibit a lattice parameter distribution centered at compressive strain $\varepsilon_{InAs\text{-}memb} = 1.00 \pm 0.05\%$ with respect to bulk InAs. We attribute the second ensemble to islands grown on the freestanding membranes, under a remaining compressive strain driven toward the Si lattice parameter.[39] Finally, we can use Gaussian fits to the radial scans at the main

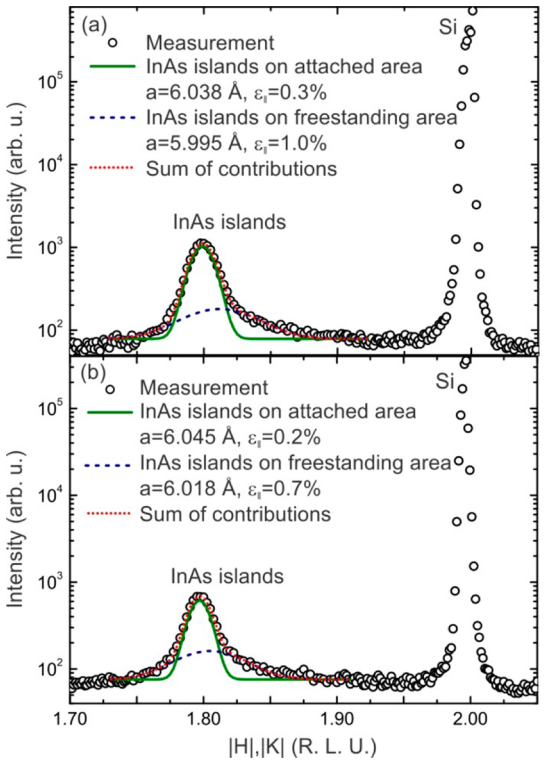

Figure 6. Radial X-ray diffraction scans for two coverages of InAs. (a) Radial scan measured on the sample with 1 ML InAs coverage. Fitting the InAs peak requires two island ensembles with different strain states. (b) Radial scan measured on the sample with 0.6 ML InAs. Again fitting the InAs peak requires two strain states.

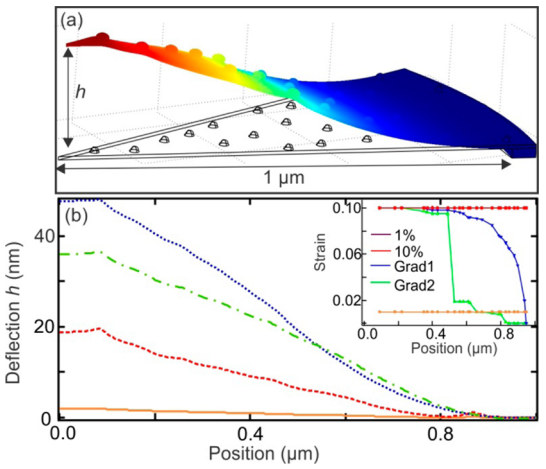

Figure 7. (a) Model of nanostressors on the section of a circular Si membrane as built for finite-element calculations, for 1 ML nominal coverage. The Si membrane is constrained along one edge. The system is depicted prior and after strain sharing between nanostressor and substrate, which elastically relaxes the compressive strain in the nanostressors and elastically transfers tensile strain to the nanomembrane substrate. Vertical deflection upon strain sharing is indicated by the color scale on the membrane surface (blue to red: no deflection to maximum deflection *h*): the substrate becomes longer because of tensile strain. (b) Nanomembrane deflection profiles as a function of distance from the constrained edge. Four deflection profiles are obtained corresponding to four different lateral strain distributions among the islands, as depicted in the inset (two with constant strain and two with changing strain as a function of the position on the island).

position of the two island ensembles to estimate the strain distribution of the island ensemble centered at (*h*,*k*) reciprocal-space positions near 1.8 (therefore corresponding to smaller lattice parameters with respect to InAs bulk). For islands on the freestanding membrane, we deduce from the Gaussian width of the smaller, broader peak in Figure 6 that an island strain distribution of ±2.7% can be found for the islands at the bent areas of the freestanding nanomembranes; hence the strain in the islands varies from 2.35% compressive to 0.35% tensile strain for this ensemble. Similar results are obtained for the second sample with 0.6 ML InAs deposited (Figure 6b). We can decompose, as for the 1 ML data, the InAs island peak into two contributions (green solid and blue dashed lines in Figure 6b), indicating $\varepsilon_{\text{InAs-relaxed}} = 0.2\%$ and $\varepsilon_{\text{InAs-memb}} = 0.7\%$ (6.045 and 6.018 Å) compressive strain (lattice parameter) for flat areas and membrane areas, respectively. The island strain $\varepsilon_{\text{InAs-memb}} = 0.7\%$ agrees with the strain transferred to the Si membrane of $\varepsilon_{\text{Si}} = 0.29\%$.[40] Gaussian fits to the radial XRD scans at the peak position corresponding to the InAs islands on the nanomembrane indicate an island strain distribution of ±2.5% for this 0.6 ML sample. Therefore, the strain varies from 1.95% compressive to 0.55% tensile.

X-ray diffraction results unambiguously indicate that part of the InAs island population is strained by an average $\varepsilon_{\text{InAs-memb}} = 0.7\%$ to 1% compressive strain. The ±2.5−2.7% strain distribution that we determine centered at this condition requires further interpretation. The strain distribution may either originate from strong lattice parameter gradients inside each island on the freestanding areas or indicate that each island has an average strain that depends on its position on the nanomembrane (lateral strain distribution).

In an effort to clarify the strain distribution among the InAs islands that we deduce from the XRD results, a simple geometrical model was constructed and an FEM calculation carried out. In this model, the InAs islands act as nanostressors of the Si membrane by introducing an interface strain between the nanostressor and the membrane depending on their position on the membrane.

The nanostressors are modeled to represent the InAs islands with their average diameter, height, and surface density obtained from the AFM image for the sample with 1 ML InAs deposited. To minimize computation times, only part of the membrane was constructed, using periodic boundary conditions and taking advantage of the nearly circular shape of the bent areas as seen in Figure 3. The model is illustrated in Figure 7a. In our analysis we considered four different initial lateral strain distributions of the InAs islands *versus* distance from the free-hanging edge of the membrane. First, we assume a constant strain of 1% for all islands with

respect to the Si membrane (the average strain determined by XRD, hence islands are partly relaxed). Second, we assume a fixed 10% strain between island and membrane (equal to fully coherent islands). Finally, we observe two cases in which the strain between islands and membrane changes according to the island position with respect to the membrane edge trying to modulate a lateral strain distribution. The strain distributions from the center of the nanomembrane to the fixed edge is depicted in the inset of Figure 7b, showing the strain of each island (islands connected by the solid lines) as a function of their position on the membrane. In a second step, the system is allowed to relax into its continuum mechanical equilibrium. This elastic relaxation results in an upward bending of the thin membrane upon transfer of strain from the nanostressors to the compliant substrate.

The deflection profiles of the Si membrane obtained for the four simulated strain distributions are plotted in Figure 7b. These results show that a constant lateral strain distribution in all the nanostressors yields a relatively small deflection (*i.e.*, $h < 20$ nm) of the membrane, whereas larger bending is achieved when there is a position-dependent lateral strain distribution among the islands on the membrane.

We ascribe this behavior to the following: a strain transfer between the compressive strained nanostressor and the membrane leads to a tensile strain of the membrane. This strain results in a convex curvature (seen from the top) of the freestanding membrane (as depicted in Figure 8 schematically). In the middle of the membrane, where there are no constraints, the membrane bends up, providing an overall convex shape, as observed in the AFM as well as in the FEM simulations. Near the clamped edges, where the membrane is fixed to the substrate, a convex curvature would result in a down bending of the membrane. Indeed, a lateral strain distribution with a high interfacial strain between nanostressor/membrane results in a down bending of the membrane (see Supporting Information). Furthermore, the up bending results in a concave curvature of the edges of the clamped membrane. This curvature compresses the nanostressor in this area and cannot relax some of their strain as in the middle of the membrane. Both effects lead to the observation of the FEM results that a membrane with a constant lateral strain distribution shows a smaller deflection than a membrane with a position-dependent strain distribution.

From these results, we conclude that a constant initial strain cannot explain the observed bending height h of about 100 nm seen in the AFM profiles depicted in Figure 3c and d. Indeed, for a fixed strain of 1% for all islands on the freestanding membrane, h is only a few nanometers (orange, solid curve in Figure 7b). Even with a maximal strain assuming fully coherent islands on top of the Si membrane, *i.e.*, having all nanostressors with 10% interfacial strain, the maximal h barely exceeds

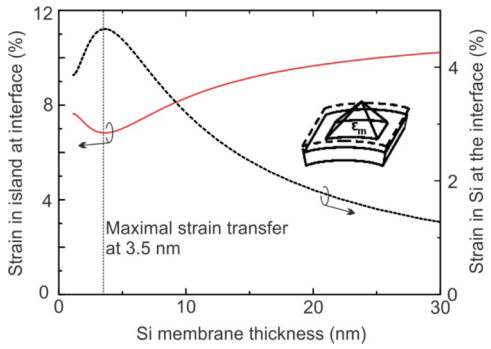

Figure 8. Strain at the interface in a freestanding Si nanomembrane (black dotted line) as well as in the InAs island (red solid line) as a function of nanomembrane thickness. The equivalent nominal 2D-layer InAs coverage over the considered area, indicated by the dashed line in the inset, is calculated by taking into account the 3D island geometry.

~20 nm (red, dashed curve in Figure 7b). This indicates that a uniform strain distribution of the InAs island ensemble, *e.g.*, arising from the mismatch in thermal expansion coefficients, is most likely not responsible for the observed bending of the membrane.

Consequently, a lateral strain distribution depending on the nanostressor position on the membrane gives rise to a value $h > 45$ nm (green, dash-dotted curve and blue, dotted curve in Figure 7b). The best lateral strain distributions we find—describing the observed bending semiquantitatively—exhibit a strain profile with the nanostressor/membrane interfaces highly strained at the freestanding membrane center and decreasing when moving toward the membrane edges. These results indicate that during island formation the InAs islands can transfer some of their strain to the membrane, when they are formed in the middle, where the membrane is most compliant, whereas they plastically relax near the edges of the membrane, most likely due to bonding of the membrane to the edge, which makes it more rigid. Taking into account that the material deposition is rather slow, because of the low growth rate (0.01 ML/s), large parts of the deposition will happen on a slightly prebent membrane. Here, the convex center will promote more coherent growth, whereas the concave areas on the edges will promote island relaxation. This difference in formation behavior as well as a potential prebending should give rise to the observed differences in the island height distribution and density observed in Figures 3 and 4 as well as the strain distribution observed in the XRD experiments.

As our experimental results in conjunction with the FEM analysis indicate that the InAs islands can introduce strain into the freestanding membrane, we finally address the question of the maximum possible strain transfer from the stressor to the compliant substrate. This analysis should also tell if enough strain can be transferred to allow coherent InAs island growth on freestanding Si membranes. For simplicity, we perform continuum elasticity calculations as done for Ge islands on Si.[25,41]

Figure 8 shows the calculated strain in an InAs island at the interface with a Si compliant substrate as function of the Si thickness (red solid curve). Alternatively, we can also plot the strain in Si at the interface (black dotted line in Figure 8), in order to show the amount of strain transferred into the Si from the InAs island.

Obviously, most of the misfit stain (~10%) is still located inside the InAs island when the Si layer is 30 nm thick (red solid line in Figure 8). (The InAs island would certainly dislocate under those conditions.) The amount of misfit strain in the InAs island decreases with decreasing Si substrate thickness and reaches a minimum of ~6.8% for a 3.5 nm thick Si membrane.

Our calculation indicates that there is a larger possibility of formation of dislocations in the InAs islands when they are grown on a thick Si membrane, due to the reduced strain transfer. Conversely, the strain left in the island can be transferred to the Si when the Si becomes thinner (<30 nm). For instance, Figure 8 shows that the InAs island can share ~1.5% misfit strain with 25 nm thick Si, whereas it can share ~3.3% misfit strain with 10 nm thick Si. With the thickness of our current Si substrates only one-third of the strain buildup in the islands is shared with the substrate, although a condition of partially coherent epitaxy is obtained.

Finally, Figure 8 indicates that a 3.5 nm thick Si membrane can accommodate ~4.5% misfit strain and leave ~7% strain in the InAs island, a value for which fully coherent epitaxy may be possible. Indeed, there should be no fundamental limitations to produce 3.5 nm thin membranes. We would like to point out that thin Si membranes of 6 nm were used in folded and rolled-up nanotubes, showing the stability of the material,[42] and no fundamental limit was encountered. Furthermore, for other semiconductor materials three-dimensional structures out of sub-nanometer layers (0.43 nm) were formed and proved mechanically stable.[43] As Si NMs have been made thinner than 2 nm,[44] we think it is possible to make them freestanding over small areas or as cantilevers. Our current experiments show that for our samples and growth strategy this ideal state is not reached. We achieve a partial strain sharing of the islands formed on the compliant freestanding membrane, whereas the islands on the rigid part are fully relaxed.

CONCLUSIONS

In this work, freestanding, but edge-supported Si nanomembranes were produced by selectively underetching patterned SOI substrates. These freestanding membranes were used as compliant substrates for InAs growth using MBE. Various amounts of InAs were deposited on to the substrate, and the resulting InAs nanostructures were characterized by SEM, AFM, and XRD. Our SEM investigation shows that Si membranes as thin as 10 nm can be overgrown in a III–V MBE, staying intact and freestanding. SEM as well as AFM shows the typical island formation observed for InAs on Si with slight modifications at freestanding-membrane (compliant substrate) areas. The AFM investigation shows a bending up of the freestanding membrane of up to 100 nm after island growth. From the degree of bending an average global biaxial strain of the Si membrane of *ca.* 0.3% is calculated. Changes in island density on the freestanding parts point to modifications in the wetting or diffusion behavior of the InAs on the compliant substrate. XRD indicates that the InAs can transfer some strain to the ultrathin membrane, giving rise to the observed bending. Detailed investigations of the diffraction reveal an average strain of 0.7–1% of InAs islands on the freestanding membrane, as well as an observable strain distribution for the island ensemble on the membrane of ±2.5%. FEM calculations suggest that the distribution of strain among islands arises from a position-dependent strain of the islands across the freestanding membrane. Finally, continuum elasticity calculations suggest that for thin enough Si nanomembranes coherent InAs growth could be possible through strain sharing, in spite of the low chemical affinity of InAs for Si. Our results indicate that nanomembranes could pave the way for coherent growth of III–V material on Si substrates. The results presented here open the possibility of a local, nanometer-scale tailoring of the band structure of Si nanomembranes by imposing strain *via* heteroepitaxy of nanostressors, islands of compounds with reduced chemical affinity with respect to the standard Si/Ge approach. Suitable candidates that could lead to highly strained membranes are InP (8% strain), GaSb (12.2% strain), and InSb (19.3% strain) among the III–Vs and CdS (7% strain) and CdTe (19.2% strain) among the most common cubic II–VI compounds.

METHODS

Sample Preparation and Growth. The top silicon layer (the "template" layer) of a SOI wafer was thinned to a final thickness of 10, 15, and 20 nm and afterward patterned by optical lithography with square structures of a size ranging from $20 \times 20\ \mu m^2$ down to $4 \times 4\ \mu m^2$. Before growth, samples were cleaned by etching them several times in H_2SO_4/H_2O_2 (1:3) and HF (3 vol %) for 10 and 3 min, respectively. Finally, an etching step of 10–15 min in HF (10 vol %) was carried out to obtain a H-passivated surface as well as to underetch the SiO_2 of the SOI wafer *ca.* 1 μm laterally, leaving effectively a cantilever. As the ultrathin top Si layer contains defects (pinholes), this step also gives rise to circular underetched areas (see Figure 1 for the process). After cleaning and underetching, samples were immediately introduced into the loadlock chamber of the III–V MBE (Omicron) at IFW Dresden. Following recipes from the

literature,[30,31] the hydrogen passivating the Si surface was thermally desorbed, and a streaky (2 × 1) reflection high-energy electron diffraction pattern was observed after 10 min annealing at about 50 °C below the desorption temperature. Samples were cooled to 400 °C and exposed for 2 min to an As-flux (beam equivalent pressure about 1×10^{-5} mbar). Different amounts of InAs were then deposited with a growth rate of 0.01 ML/s for each sample. A transition from a streaky RHEED pattern to a "spotty" pattern was observed after *ca.* 30 s of growth (*ca.* 0.3 ML) for all samples. After reaching the final thickness, the substrate was quenched (at a rate greater than 30 °C/s) to 100 °C. Before all growth runs, InAs rates were calibrated by growth on GaAs (001) using RHEED oscillations of InGaAs layers as well as InAs island formation time on the GaAs (001) surface.[45]

Scanning Electron Microscopy and Atomic Force Microscopy. Scanning electron microscopy was carried out with a Zeiss nVision at the IFW Dresden at 20 kV. To obtain a better contrast, the samples were tilted 53°. Images were taken with the secondary electron detector as well as with the in-lens detector at various magnifications. Atomic force microscopy was carried out with a DI Multimode Nanoscope IIIa of the LNNano (Campinas, Brazil). Great care was taken to ensure a dry sample environment to suppress tip artifacts and get a correct impression of the sample topology. Images were processed using the free AFM software Gwyddion as well as our own written software XIm.

X-ray Diffraction. Grazing-incidence X-ray diffraction measurements were carried out at the XRD2 beamline of the Brazilian Synchrotron Light Laboratory (LNLS-Campinas) at an energy of 10.2 keV using a 4+2-circle diffractometer. An incidence angle of 0.16° and a linear detector integrating exit angles from 0° to 1.5° were used. Samples with different InAs coverages were investigated, and reciprocal-space maps in the vicinity of the (220) silicon reflection were used to retrieve the strain state of the deposited InAs islands.

Finite Element Modeling and Continuum Mechanical Calculation. We used a commercial finite element method software package to simulate the strain induced by InAs nanostressors in the Si nanomembrane. Taking advantage of the radial symmetric geometry of the freestanding areas of the sample the simulations were restricted to a sector of the structure assuming symmetric boundary conditions, *i.e.*, (1) no displacement is allowed in the direction perpendicular to the plane of symmetry; (2) no rotation is allowed in the direction parallel to the plane of symmetry. Hereby, the membrane is fixed on the one side to the substrate and can relax freely in the middle. Nanostressors with morphology and size estimated from the AFM results were distributed with an island density similar to the one observed experimentally. The interface between the nanostressor (InAs island) and the freestanding, edge-supported silicon membrane was strained using the nominal lattice mismatch between InAs and Si. Hence the islands are assumed coherent to the Si membrane, as this provides maximum stress. In the next step, the structure is allowed to relax into its mechanical equilibrium and the bending height h of the structure was obtained. Out-of-plane displacement profiles were then extracted and compared semiquantitatively to the bending observed in our nanomembranes.

The elastic strain sharing at the Si and InAs interface can be estimated by continuum-mechanics calculations using a modified Timoshenko's formula. These calculations are performed using a 2D coverage equivalent to an island with the geometry shown in the inset of Figure 8.

Conflict of Interest: The authors declare no competing financial interest.

Acknowledgment. We thank V. L. Pimentel (LNNano) and L. A. Farias (LNNano) for their help with the AFM. We acknowledge fruitful discussions with and experimental help from P. Atkinson (IFW), S. Baunack (IFW), and A. Brandt (IFW). T. Gemming (IFW) provided access to TEM; we thank J. Thomas (IFW) for helping us use the instrument. M.H.H. thanks F. Liu (UU) for helpful discussions on continuum-mechanics calculations. X. Li (UIUC) made early CVD depositions for the same system to investigate InAs ordering behavior. Work performed at the University of Wisconsin−Madison (F.C., M.H.H., and M.G.L.) was supported by DOE, Grant No. DE-FG02-03ER46028. Work carried out in Dresden was supported by a Multidisciplinary University Research Initiative (MURI) sponsored by the U.S. Air Force Office of Scientific Research (AFOSR) Grant No. FA9550-09-1-0550. Financial support by FAPESP (Project 2011/22945-1) is acknowledged. Beamtime was granted by the LNLS under proposal number D10A XRD2-10919.

Supporting Information Available: Additional FEM calculations as well as cross-section TEM images of the freestanding membranes (with an island) are presented. This material is available free of charge *via* the Internet at http://pubs.acs.org.

REFERENCES AND NOTES

1. Rogers, J. A.; Lagally, M. G.; Nuzzo, R. G. Synthesis, Assembly and Applications of Semiconductor Nanomembranes. *Nature* **2011**, *477*, 45–53.
2. Scott, S. A.; Lagally, M. G. Elastically Strain-Sharing Nanomembranes: Flexible and Transferable Strained Silicon and Silicon-Germanium Alloys. *J. Phys. D: Appl. Phys.* **2007**, *40*, R75–R92.
3. Rogers, J. A.; Someya, T.; Huang, Y. G. Materials and Mechanics for Stretchable Electronics. *Science* **2010**, *327*, 1603–1607.
4. Huang, M. H.; Cavallo, F.; Liu, F.; Lagally, M. G. Nanomechanical Architecture of Semiconductor Nanomembranes. *Nanoscale* **2011**, *3*, 96–120.
5. Rogers, J. A. Slice and Dice, Peel and Stick: Emerging Methods for Nanostructure Fabrication. *ACS Nano* **2007**, *1*, 151–153.
6. Roberts, M. M.; Klein, L. J.; Savage, D. E.; Slinker, K. A.; Friesen, M.; Celler, G.; Eriksson, M. A.; Lagally, M. G. Elastically Relaxed Free-Standing Strained-Silicon Nanomembranes. *Nat. Mater.* **2006**, *5*, 388–393.
7. Malachias, A.; Mei, Y. F.; Annabattula, R. K.; Deneke, C.; Onck, P. R.; Schmidt, O. G. Wrinkled-up Nanochannel Networks: Long-Range Ordering, Scalability, and X-Ray Investigation. *ACS Nano* **2008**, *2*, 1715–1721.
8. Feng, X.; Yang, B. D.; Liu, Y. M.; Wang, Y.; Dagdeviren, C.; Liu, Z. J.; Carlson, A.; Li, J. Y.; Huang, Y. G.; Rogers, J. A. Stretchable Ferroelectric Nanoribbons with Wavy Configurations on Elastomeric Substrates. *ACS Nano* **2011**, *5*, 3326–3332.
9. Wang, S. D.; Xiao, J. L.; Song, J. Z.; Ko, H. C.; Hwang, K. C.; Huang, Y. G.; Rogers, J. A. Mechanics of Curvilinear Electronics. *Soft Matter* **2010**, *6*, 5757–5763.
10. Wu, J. A.; Li, M.; Chen, W. Q.; Kim, D. H.; Kim, Y. S.; Huang, Y. G.; Hwang, K. C.; Kang, Z.; Rogers, J. A.; Strain-Isolation, A. Design for Stretchable Electronics. *Acta Mech. Sin.* **2010**, *26*, 881–888.
11. Kim, D. H.; Kim, Y. S.; Wu, J.; Liu, Z. J.; Song, J. Z.; Kim, H. S.; Huang, Y. G. Y.; Hwang, K. C.; Rogers, J. A. Ultrathin Silicon Circuits with Strain-Isolation Layers and Mesh Layouts for High-Performance Electronics on Fabric, Vinyl, Leather, and Paper. *Adv. Mater.* **2009**, *21*, 3703–3707.
12. Shir, D.; Yoon, J.; Chanda, D.; Ryu, J. H.; Rogers, J. A. Performance of Ultrathin Silicon Solar Microcells with Nanostructures of Relief Formed by Soft Imprint Lithography for Broad Band Absorption Enhancement. *Nano Lett.* **2010**, *10*, 3041–3046.
13. Yoon, J.; Baca, A. J.; Park, S. I.; Elvikis, P.; Geddes, J. B.; Li, L. F.; Kim, R. H.; Xiao, J. L.; Wang, S. D.; Kim, T. H.; *et al.* Ultrathin Silicon Solar Microcells for Semitransparent, Mechanically Flexible and Microconcentrator Module Designs. *Nat. Mater.* **2008**, *7*, 907–915.
14. Yuan, H.-C.; Shin, J.; Qin, G.; Sun, L.; Bhattacharya, P.; Lagally, M. G.; Celler, G. K.; Ma, Z. Flexible Photodetectors on Plastic Substrates by Use of Printing Transferred Single-Crystal Germanium Membranes. *Appl. Phys. Lett.* **2009**, *94*, 013102.
15. Rastelli, A.; Ding, F.; Plumhof, J. D.; Kumar, S.; Trotta, R.; Deneke, C.; Malachias, A.; Atkinson, P.; Zallo, E.; Zander, T.; *et al.* Controlling Quantum Dot Emission by Integration of Semiconductor Nanomembranes onto Piezoelectric Actuators. *Phys. Status Solidi B* **2012**, *249*, 687–696.

16. Ko, H.; Takei, K.; Kapadia, R.; Chuang, S.; Fang, H.; Leu, P. W.; Ganapathi, K.; Plis, E.; Kim, H. S.; Chen, S. Y.; *et al*. Ultrathin Compound Semiconductor on Insulator Layers for High-Performance Nanoscale Transistors. *Nature* **2010**, *468*, 286–289.
17. Prinz, V. Y.; Seleznev, V. A.; Gutakovsky, A. K.; Chehovskiy, A. V.; Preobrazhenskii, V. V.; Putyato, M. A.; Gavrilova, T. A. Free-Standing and Overgrown InGaAs/GaAs Nanotubes, Nanohelices and Their Arrays. *Phys. E (Amsterdam, Neth.)* **2000**, *6*, 828–831.
18. Schmidt, O. G.; Schmarje, N.; Deneke, C.; Muller, C.; Jin-Phillipp, N. Y. Three-Dimensional Nano-Objects Evolving from a Two-Dimensional Layer Technology. *Adv. Mater.* **2001**, *13*, 756–759.
19. Deneke, C.; Songmuang, R.; Jin-Phillipp, N. Y.; Schmidt, O. G. The Structure of Hybrid Radial Superlattices. *J. Phys. D: Appl. Phys.* **2009**, *42*, 103001.
20. Cavallo, F.; Lagally, M. G. Semiconductors Turn Soft: Inorganic Nanomembranes. *Soft Matter* **2010**, *6*, 439–455.
21. Ritz, C. S.; Kim-Lee, H. J.; Detert, D. M.; Kelly, M. M.; Flack, F. S.; Savage, D. E.; Cai, Z.; Evans, P. G.; Turner, K. T.; Lagally, M. G. Ordering of Nanostressors on Free-Standing Silicon Nanomembranes and Nanoribbons. *New J. Phys.* **2010**, *12*, 103011.
22. Huang, M. H.; Ritz, C. S.; Novakovic, B.; Yu, D. C.; Zhang, Y.; Flack, F.; Savage, D. E.; Evans, P. G.; Knezevic, I.; Liu, F.; *et al*. Mechano-Electronic Superlattices in Silicon Nanoribbons. *ACS Nano* **2009**, *3*, 721–727.
23. Kim-Lee, H. J.; Savage, D. E.; Ritz, C. S.; Lagally, M. G.; Turner, K. T. Control of Three-Dimensional Island Growth with Mechanically Responsive Single-Crystal Nanomembrane Substrates. *Phys. Rev. Lett.* **2009**, *102*, 226103.
24. Zhang, P. P.; Yang, B.; Rugheimer, P. P.; Roberts, M. M.; Savage, D. E.; Liu, F.; Lagally, M. G. Influence of Germanium on Thermal Dewetting and Agglomeration of the Silicon Template Layer in Thin Silicon-on-Insulator. *J. Phys. D: Appl. Phys.* **2009**, *42*, 175309.
25. Huang, M. H.; Rugheimer, P.; Lagally, M. G.; Liu, F. Bending of Nanoscale Ultrathin Substrates by Growth of Strained Thin Films and Islands. *Phys. Rev. B* **2005**, *72*, 085450.
26. Rim, K.; Chi, J.; Chen, H.; Jenkins, K. A.; Kanarsky, T.; Lee, K.; Mocuta, A.; Zhu, H.; Roy, R.; Newbury, J. *Characteristics and Device Design of Sub-100nm Strained Si N- and PMOSFETs. Symposium on VLSI Technology Proceedings*; IEEE, 2002, DOI: 10.1109/VLSIT.2002.1015406.
27. Sánchez-Pérez, J. R.; Boztug, C.; Chen, F.; Sudradjat, F. F.; Paskiewicz, D. M.; Jacobson, R.; Lagally, M. G.; Paiella, R. Direct-Bandgap Light-Emitting Germanium in Tensilely Strained Nanomembranes. *Proc. Natl. Acad. Sci.* **2011**, *108*, 18893–18898.
28. Gill, S. P. A. An Analytical Model for the Growth of Quantum Dots on Ultrathin Substrates. *Appl. Phys. Lett.* **2011**, *98*, 161910.
29. Ni, Y.; He, L. H. Spontaneous Formation of Vertically Anti-correlated Epitaxial Islands on Ultrathin Substrates. *Appl. Phys. Lett.* **2010**, *97*, 261911.
30. Cirlin, G. E.; Dubrovskii, V. G.; Petrov, V. N.; Polyakov, N. K.; Korneeva, N. P.; Demidov, V. N.; Golubok, A. O.; Masalov, S. A.; Kurochkin, D. V.; Gorbenko, O. M.; *et al*. Formation of InAs Quantum Dots on a Silicon (100) Surface. *Semicond. Sci. Technol.* **1998**, *13*, 1262–1265.
31. Mano, T.; Fujioka, H.; Ono, K.; Watanabe, Y.; Oshima, M. InAs Nanocrystal Growth on Si (100). *Appl. Surf. Sci.* **1998**, *130*, 760–764.
32. Zhao, Z. M.; Hulko, O.; Yoon, T. S.; Xie, Y. H. Initial Stage of InAs Growth on Si(001) Studied by High-Resolution Transmission Electron Microscopy. *J. Appl. Phys.* **2005**, *98*, 123526.
33. Alzoubi, T.; Usman, M.; Benyoucef, M.; Reithmaier, J. P. Growth of Inas Quantum Dots and Dashes on Silicon Substrates: Formation and Characterization. *J. Cryst. Growth* **2011**, *323*, 422–425.
34. Jha, S.; Song, X.; Babcock, S. E.; Kuech, T. F.; Wheeler, D.; Wu, B.; Fay, P.; Seabaugh, A. Growth of InAs on Si Substrates at Low Temperatures Using Metalorganic Vapor Phase Epitaxy. *J. Cryst. Growth* **2008**, *310*, 4772–4775.
35. Pimpinelli, A.; Villain, J. *Physics of Crystal Growth*; University Press: Cambridge, 1998.
36. Rastelli, A.; Känel, H. v. Surface Evolution of Faceted Islands. *Surf. Sci.* **2002**, *515*, L493–L498.
37. Ewald, P. P. Die Intensität der Interferenzflecke bei Zinkblende und das Gitter der Zinkblende. *Ann. Phys.* **1914**, *349*, 257–282.
38. Kegel, I.; Metzger, T. H.; Lorke, A.; Peisl, J.; Stangl, J.; Bauer, G.; Nordlund, K.; Schoenfeld, W. V.; Petroff, P. M. Determination of Strain Fields and Composition of Self-Organized Quantum Dots Using X-Ray Diffraction. *Phys. Rev. B* **2001**, *63*, 035318.
39. Malachias, A.; Magalhães-Paniago, R.; Neves, B. R. A.; Rodrigues, W. N.; Moreira, M. V. B.; Pfannes, H.-D.; de Oliveira, A. G.; Kycia, S.; Metzger, T. H. Direct Observation of the Coexistence of Coherent and Incoherent InAs Self-Assembled Dots by X-Ray Scattering. *Appl. Phys. Lett.* **2001**, *79*, 4342–4344.
40. Making the simple assumption that $E_{InAs}\varepsilon_{InAs} = E_{Si}\varepsilon_{Si}$, with E as elastic moduli. The calculation (using $E_{InAs} = 5.14 \times 10^{-11}$ dyn/cm^2 and $E_{Si} = 13 \times 10^{-11}$ dyn/cm^2) yields an error of 7%.
41. Liu, F.; Huang, M. H.; Rugheimer, P. P.; Savage, D. E.; Lagally, M. G. Nanostressors and the Nanomechanical Response of a Thin Silicon Film on an Insulator. *Phys. Rev. Lett.* **2002**, *89*, 136101.
42. Prinz, V. Y.; Grützmacher, D.; Beyer, A.; David, C.; Ketterer, B.; Deckardt, E. A New Technique for Fabricating Three-Dimensional Micro- and Nanostructures of Various Shapes. *Nanotechnology* **2001**, *12*, 399–402.
43. Deneke, C.; Schmidt, O. G. Structural Characterization and Potential X-Ray Waveguiding of a Small Rolled-up Nanotube with a Large Number of Windings. *Appl. Phys. Lett.* **2006**, *89*, 123121.
44. Chen, F.; Ramayya, E. B.; Euaruksakul, C.; Himpsel, F. J.; Celler, G. K.; Ding, B.; Knezevic, I.; Lagally, M. G. Quantum Confinement, Surface Roughness, and the Conduction Band Structure of Ultrathin Silicon Membranes. *ACS Nano* **2010**, *4*, 2466–2474.
45. Arthur, J. R. Molecular Beam Epitaxy. *Surf. Sci.* **2002**, *500*, 189–217.